CrystEngComm

Simple One-pot Synthesis of Cu4SnS4 Nanoplates and Temperature-Induced Phase Transformation Mechanism

Journal:	*CrystEngComm*
Manuscript ID	CE-ART-11-2019-001772.R1
Article Type:	Paper
Date Submitted by the Author:	08-Jan-2020
Complete List of Authors:	Zhang, Xiaoyan; Nanjing Tech University, State Key Laboratory of Material-Oriented Chemical Engineering, College of Chemical Engineering Tang, Yu; Nanjing Tech University, State Key Laboratory of Material-Oriented Chemical Engineering, College of Chemical Engineering Wang, Yifeng; Nanjing Tech University, College of Materials Science and Engineering Shen, Liming; Nanjing Tech University, State Key Laboratory of Material-Oriented Chemical Engineering, College of Chemical Engineering Gupta, Arunava; University of Alabama, Centre for Materials for Information Technology Bao, Ningzhong; Nanjing Tech University, State Key Laboratory of Material-Oriented Chemical Engineering, College of Chemical Engineering; Jiangnan Graphene Research Institute,

Table of Contents Image

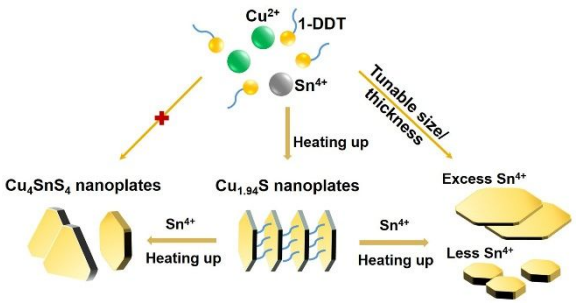

A simple one-pot heat-up method has been developed to synthesize Cu_4SnS_4 nanoplates with highly exposed (002) surfaces.

Simple One-pot Synthesis of Cu_4SnS_4 Nanoplates and Temperature-Induced Phase Transformation Mechanism

Xiaoyan Zhang[a], Yu Tang[a], Yifeng Wang[c], Liming Shen[a], Arunava Gupta[b], Ningzhong Bao[a,d*]

[a] *State Key Laboratory of Material-Oriented Chemical Engineering, College of Chemical Engineering, Nanjing Tech University, Nanjing, Jiangsu 210009, P. R. China*

[b] *Centre for Materials for Information Technology, The University of Alabama, Tuscaloosa, AL 35487, USA*

[c] *College of Materials Science and Engineering, Nanjing Tech University, Nanjing, Jiangsu 210009, China*

[d] *Jiangnan Graphene Research Institute, Changzhou, Jiangsu 213159, P. R. China*

* *To whom correspondence should be addressed:*

E-mail address: nzhbao@njtech.edu.cn

Abstract:

A simple one-pot heat-up method has been developed to synthesize Cu_4SnS_4 nanoplates with highly exposed (002) surfaces. Temperature-dependent phase transformation from monoclinic $Cu_{1.94}S$ to orthorhombic Cu_4SnS_4, and eventually to partially triclinic Cu_2SnS_3 has been observed. It revealed that the Sn^{4+} existing in the laminar structure of $Cu_{1.94}S$ nanoplates start being incorporated into the $Cu_{1.94}S$ crystal at a temperature of around 220 ^oC, and form pure orthorhombic Cu_4SnS_4 nanoplates at 260 ^oC. As the orthorhombic structure of Cu_4SnS_4 is metastable, it undergoes a phase transformation to the more stable Cu_2SnS_3 phase at a higher reaction temperature of 270 ^oC. Furthermore, the size and thickness of Cu_4SnS_4 nanoplates can be well tuned by the amount of Sn content in the initial reaction mixture to form $Cu_{1.94}S$ nanoplates. Additionally, the formation of $Cu_{1.94}S$ nanoplates is essential for the formation of pure Cu_4SnS_4 nanocrystals at a fixed reaction temperature. UV-vis and Mott-Schottky

analysis show that the as-prepared orthorhombic Cu_4SnS_4 nanoplates exhibit n-type semiconducting behavior with a band gap of about 1.65 eV. The valence and conduction band potentials have also been determined via theoretical calculations. We believe that our synthetic method and findings will be attractive for the synthesis of other copper-based chalcogenide nanoplates as well as their potential catalytic applications.

Introduction

Copper chalcogenide nanocrystals (NCs) and their multinary derivatives are an extraordinarily interesting class of materials with a wide range of attainable stable crystal phases.[1] The I-IV-VI ternary compound Cu_xSnS_y, with suitable band-gap in the range of 1-1.7 eV,[2,3] along with outstanding optical and electronic properties, is attractive for efficient solar energy conversion and storage.[3-8] Furthermore, the low-toxicity and earth-abundant composition[9] makes Cu_xSnS_y a promising semiconductor material for wide range of applications. However, the crystal structure of Cu_xSnS_y is quite complicated due to the changeable valence state of Sn and with different stoichiometry of Cu, Sn and S. In the solid state, five stable phases of ternary Cu_xSnS_y have been reported in the temperature range of 400-650 °C: Cu_4SnS_4, Cu_2SnS_3, $Cu_2Sn_3S_7$, $Cu_5Sn_2S_7$, and $Cu_{10}Sn_2S_{13}$[3,10] Amongst them, Cu_2SnS_3 is the most commonly explored phase, while Cu_4SnS_4 is emerging to be of interest for energy storage,[8,11-13] hydrogen evolution,[14] thermoelectrics[15,16] and to some extent in photovoltaics[3,5] due to its low thermal conductivity and appropriate band gap. However, it remains a challenge to control the crystal phase as well as the morphology of the products.

Bulk Cu_4SnS_4 compound is generally synthesized by solid-state reaction from stoichiometric mixtures of the elements or from Cu_2S/SnS_2 mixtures at elevated temperatures of 700-850 °C.[12,15] A few studies have reported on the synthesis of Cu_4SnS_4 nanocrystals or thin films using solvothermal/ hydrothermal processes[14,17,18] chemical bath deposition,[3,19,20] sputtering[21] *etc*. Avellaneda *et al.* prepared Cu_4SnS_4 thin films and investigated their photovoltaic applications that showed a built-in potential of 1.1 V for CdS/Cu_4SnS_4 junction.[3] Photovoltaic property of Cu_4SnS_4 has been

investigated with a power conversion efficiency of 2.34% under the standard AM 1.5 condition.[5] Furthermore, Chen *et al.* have synthesized size-controllable, oil-soluble and nearly monodisperse Cu_4SnS_4 QDs using an improved hydrothermal method with water-oil two-phase reaction system.[18] Liu *et al.* have studied the control of shapes and phases of Cu-Sn-S nanocrystals by varying both the precursors and reaction temperature.[22] Meanwhile, controllable synthesis of copper-based ternary and quaternary semiconductor nanoplates with oriented growth is of great interest to investigate their optical and photoelectrochemical properties.[23] To the best of our knowledge, the synthesis and formation mechanism of Cu_4SnS_4 nanoplates as well as their optical properties have not been previously reported.

Previously, researchers have observed that uniform $Cu_{1.94}S$ nanoplates could be obtained with Sn-X binding to the surface of nanoplates, aiding in the formation of 2D structure as well as self-assembly.[24] Further incorporation of Sn or Sn+Zn into $Cu_{1.94}S$ result in the phase transformation from $Cu_{1.94}S$ to Cu_3SnS_4[25] and Cu_2ZnSnS_4, [26] respectively. Furthermore, kuramite Cu_3SnS_4 and mohite Cu_2SnS_3 nanoplatelet have been synthesized using covellite CuS as templates.[27] Post-synthetic incorporation of Sn into copper sulfide has been shown to be an effective way of producing Cu_xSnS_y and the product is sensitive to the crystal structure of copper sulfide and the source of Sn.[25, 27] Moreover, the controllable synthesis of multinary sulfide semiconductor nanocrystals has long been investigated, with the reults demonstrating that the properties of the semiconductor is dependent on its crystal structure, morphology, composition, *etc.* [28-32] Herein, we report on our recent results on Cu_4SnS_4 nanoplates prepared by using $Cu_{1.94}S$ nanoplates as templates. Our investigation indicates that the existing Sn^{4+} in solution can be incorporated into the $Cu_{1.94}S$ nanoplates at a specific reaction temperature, resulting in the formation a new orthorhombic Cu_4SnS_4 structure. Moreover, the morphology of the resulting Cu_4SnS_4 retain the shape of the nanoplates with enlargement in the thickness. The size and thickness of the Cu_4SnS_4 nanoplates can further be tuned via changes in the initial content of Sn^{4+} during the reaction. We have investigated the structural transformation of monoclinic $Cu_{31}S_{16}$ to orthorhombic Cu_4SnS_4 and the related optical band structure of the resulting nanoplates. Our findings

can be helpful in realizing the formation of other complex chalcogenide nanoplates.

Experimental section

Materials

Copper(II) acetylacetonate ($Cu(acac)_2$, Aladdin, 97%), tin(IV) chloride pentahydrate ($SnCl_4 \cdot 5H_2O$, 99%), 1-dodecanethiol (DDT, Aladdin, 98%) were used without further purification. Other chemicals were all of analytical grade.

Synthesis of Cu_4SnS_4 nanoplates

All the experiments were carried out in a fume hood under inert N_2 atmosphere using standard Schlenk techniques. The Cu_4SnS_4 nanocrystals were prepared via a simple one-pot heat-up method. In brief, 0.21 g copper(II) acetylacetonate (0.8 mmoL), and 0.14 g Tin(IV) chloride pentahydrate (0.4 mmoL) were added into a 100 mL four-neck round-bottom flask containing 20 mL 1-dodecanethiol. The mixture was stirred at room temperature for 30 min with nitrogen purging and gradually heated to 120 ^oC and kept for 20 min. Subsequently, the solution was continued to be heated to 200 ^oC and maintained for 60 min. Then, the reaction system was gradually heated up to final reaction temperatures of 220, 230, 250, 260 and 270 ^oC and maintained for 30 min. After the reaction, the mixture was cooled down to room temperature, centrifuged and washed thrice with hexane.

Characterization

The crystal structure of the products was characterized using X-ray diffraction (XRD, Rigaku-Smart Lab Advance) with Cu-Kα radiation (λ = 1.5408 Å) as the X-ray source. The morphology of the nanocrystals was studied using field-emission scanning electron microscopy (FESEM, HITACHI S-4800) and transmission electron microscopy (TEM, JEM-2100F). Copper foil with carbon film was used as substrate for TEM measurement. The UV-Vis absorption spectra were collected using a UV-Vis spectrometer (Varian Cary 300). The oxidation states of elements Cu, Sn and S present in the Cu_4SnS_4 nanoplates were characterized by X-ray photoelectron spectroscopy (XPS, Escalab

250Xi).

Electrochemical measurements

The electrochemical performance was recorded on an electrochemical analyzer (CHI 660E) in a standard three-electrode cell. The working electrode was prepared by spray-painting Cu_4SnS_4 nanoplates suspension on indium tin oxide glass (ITO) glass, followed by annealing under Ar atmosphere at 300 ^oC for 30 min. Platinum plate and saturated calomel electrode (SCE) were used as the counter electrode and reference electrode, respectively. The Mott-Schottky curve was recorded in aqueous 0.1M Na_2SO_4 at pH=7 and frequency of 1000Hz.

Results and Discussion

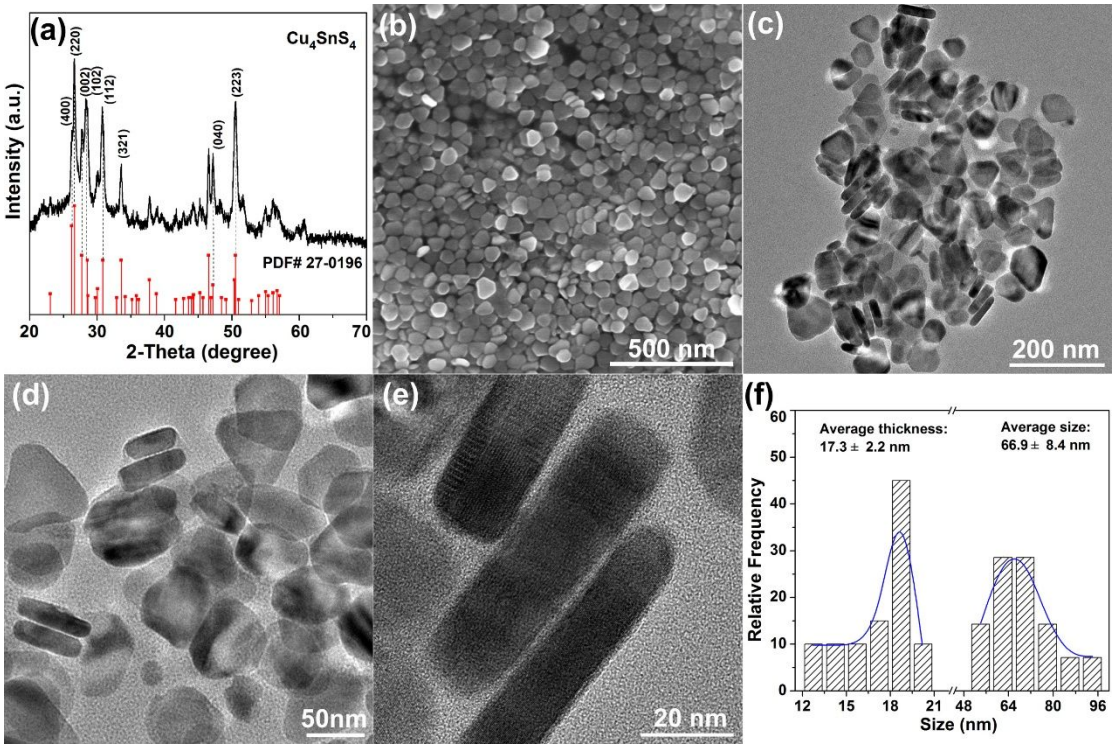

Fig. 1 (a) XRD pattern, (b) SEM, (c,d) TEM, and (e) HRTEM images of Cu_4SnS_4 nanoplates synthesized at 260 ^oC, (f) size distribution histogram of Cu_4SnS_4 nanoplates

The crystal structure and morphology of Cu_4SnS_4 nanoplates have been investigated using X-ray diffraction (XRD), scanning electron microscopy (SEM) and transmission

electron microscopy (TEM). As shown in Fig. 1a, the major diffraction peaks can well be indexed to the orthorhombic Cu_4SnS_4 (JCPDS card No. 27-0196, space group *Pnma* (62), *a*=13.57, *b*=7.69, *c*=6.42 Å). As shown in Fig 1b and c, uniform nanoplates are observed both in the SEM and TEM images over a large area, indicating homogenous growth of Cu_4SnS_4 nanoplates using the as-formed $Cu_{1.94}S$ nanoplates [24, 26] as template. The nanoplates are formed mostly with triangular and hexagonal shapes, with some nanoplates oriented perpendicular to the substrate (Fig. 1d and e). The three-dimensional micrograph of nanoplates could also been seen from different perspective in the TEM image (Fig. S1). As shown in the size distribution histogram of Cu_4SnS_4 nanoplates (Fig. 1f), the lateral size and thickness of individual nanoplates is about 66.9±8.4 nm and 17.3±2.2 nm, respectively. The thickness of Cu_4SnS_4 nanoplates is about twice the thickness of $Cu_{1.94}S$ nanoplates (lateral size of 55.1 ± 4.2 nm and thickness of 8.1 ±0.7 nm),[26] which further confirms the growth of Cu_4SnS_4 with incorporating Sn into the $Cu_{1.94}S$ at a reaction temperature of 260 °C.

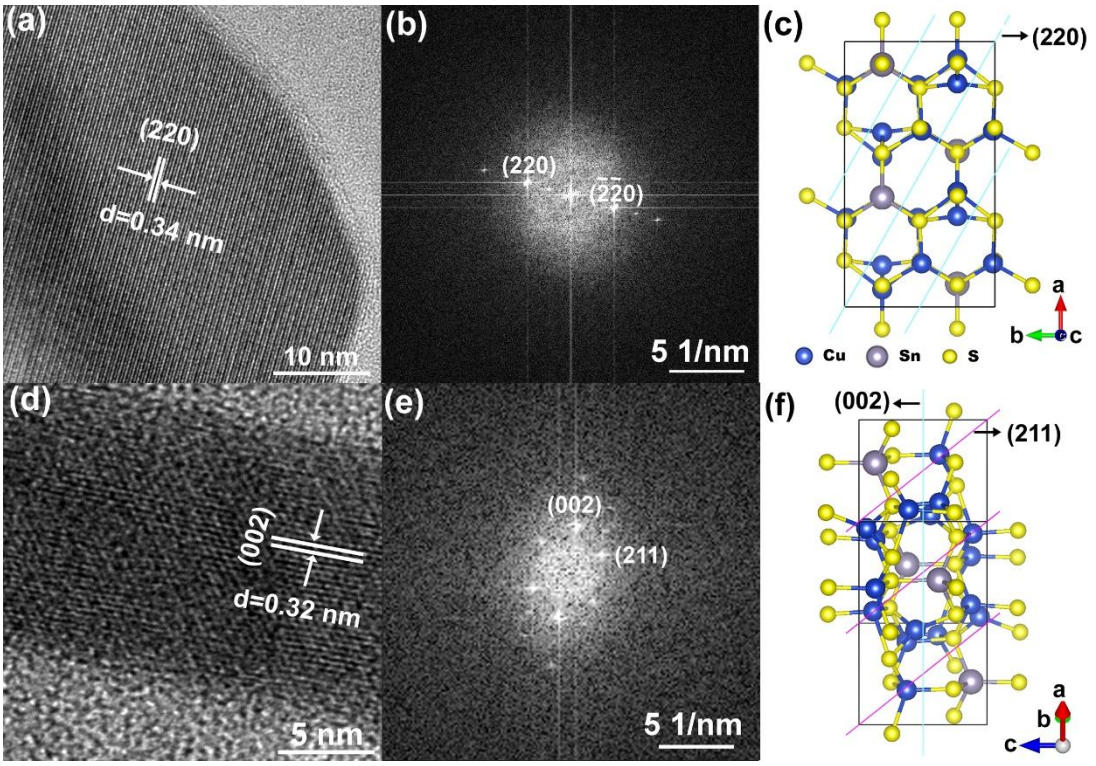

Fig. 2 HRTEM image of a Cu_4SnS_4 nanoplate (a) lying flat on the substrate, and (d) standing on end perpendicular to the substrate, (b,e) corresponding FFT images, (c,f) crystallographic model of the structure viewed from [001] and [1-20] direction,

respectively.

The HRTEM images of the Cu_4SnS_4 nanoplates lying flat on the substrate, and standing on end perpendicular to the substrate are shown in Fig. 2a and d. The lattice distance is measured to be 0.34 and 0.32 nm, corresponding to the (220) and (002) planes of Cu_4SnS_4, respectively. It also indicate that the Cu_4SnS_4 nanoplates are bound by {002} planes as the top and bottom surfaces. The corresponding fast Fourier transform (FFT) images of the lattices are shown in Fig. 2b and e, indicating the nanoplates being viewed along [001] and [1-20] direction of orthorhombic Cu_4SnS_4. The HR-TEM image (Fig. 2d) and corresponding FFT image of the side-view indicate that the nanoplates grow along the <001> direction. Fig. 2c and f illustrate the crystal structure of Cu_4SnS_4 viewed from [001] and [1-20] direction, respectively.

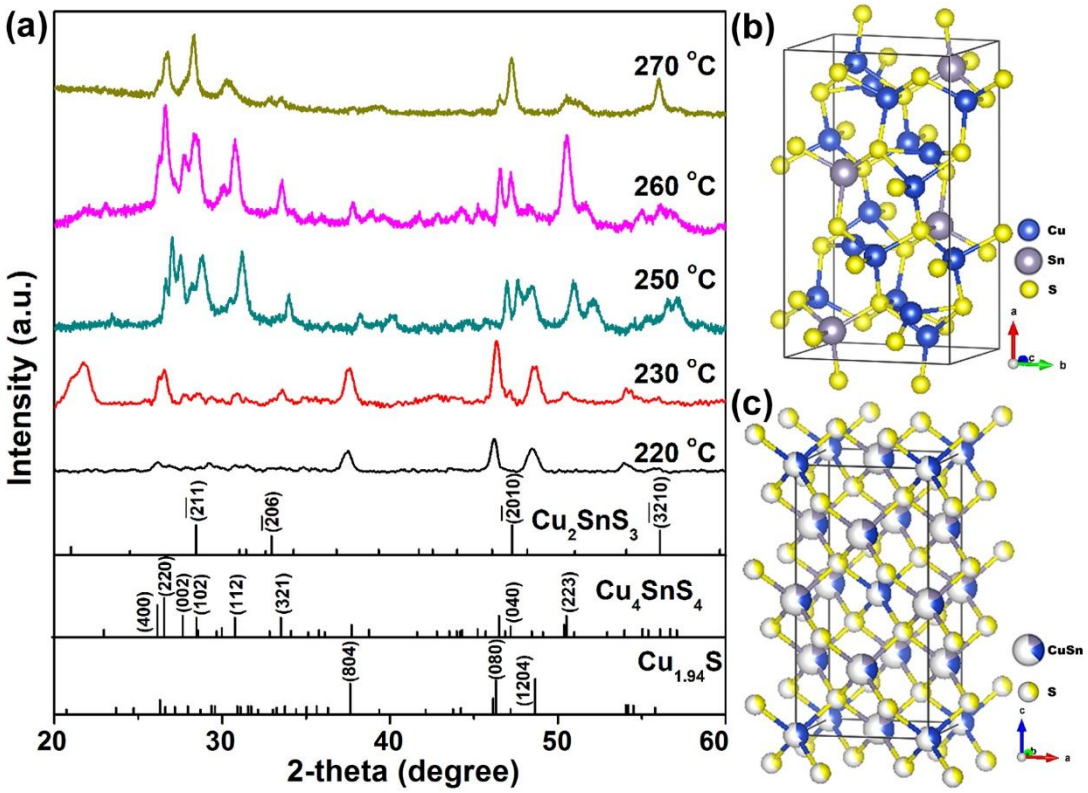

Fig. 3 (a) XRD patterns of Cu-Sn-S synthesized at different reaction temperatures, crystal structures of (b) Cu_4SnS_4 and (c) Cu_2SnS_3.

In order to investigate the formation mechanism, we have first studied the crystal structure evolution of nanocrystals synthesized at different reaction temperatures. Fig. 3 shows the XRD patterns of products synthesized at different reaction temperatures of

220, 230, 250, 260, and 270 °C, respectively. When the reaction temperature is maintained at 220 °C for 30 min, the major diffraction peaks of products are observed at 46.2 and 48.5°, which match well with the monoclinic $Cu_{1.94}S$ phase (JCPDS 34-0660). This indicates that at 220 °C, the Sn-DDT complex still exists in the laminar structure of as-formed $Cu_{1.94}S$ nanoplates. When the reaction temperature is increased to 230 °C, additional peaks at 26.3 and 26.6 ° are noticeable, which correspond to the two main diffraction peaks of orthorhombic Cu_4SnS_4 phase (JCPDS 27-0196). It demonstrates that the lowest reaction temperature for Sn^{4+} to diffuse into the $Cu_{1.94}S$ nanoplates and form Cu_4SnS_4 nanocrystals is around 230 °C. The peaks of Cu_4SnS_4 become stronger at reaction temperature of 250 °C. Note that, there exists an extra peak at 27.5 °, which can be ascribed to a trace amount of orthorhombic Cu_3SnS_4 (JCPDS 36-0217) existing in the products. The extra peak disappears at 260 °C, and all the observed peaks match well with orthorhombic Cu_4SnS_4 phase (JCPDS 27-0196), indicating the formation of phase-pure Cu_4SnS_4 nanocrystals at this temperature. Interestingly, with even higher reaction temperature of 270 °C, higher intensity of peaks at 28.3, 47.2, 56.0 ° are observed, which correspond to the (211) (2010) and (3210) planes of triclinic Cu_2SnS_3 (JSPDS 27-0198). Thus, during the simple heating up process of the reaction system from 200 to 270 °C, we have observed two distinct phase transformation processes, that is from monoclinic $Cu_{1.94}S$ to orthorhombic Cu_4SnS_4, and finally partial transformation to Cu_2SnS_3. The corresponding crystal structures of Cu_4SnS_4 and Cu_2SnS_3 are shown in Fig. 3b and c.

We have analyzed the phase transformation mechanism based on the crystal structures. The lattice parameters of three structures are summarized in Table 1.

Table 1 Lattice parameters of three crystal structures

Formula	**Structure**	**Space group**	***a*/ Å**	***b*/ Å**	***c*/ Å**	**Angle/°**
$Cu_{1.94}S$	monoclinic	P21/n (14)	26.897	15.745	13.465	90×90.13×90
Cu_4SnS_4	orthorhombic	Pnma (62)	13.57	7.69	6.42	90×90×90
Cu_2SnS_3	triclinic	P1 (1)	6.64	11.51	19.93	90×109.75×90

Djurleite ($Cu_{1.94}S$) is a semiconducting metal chalcogenide compound with a cationic deficiency structure. The space group of $Cu_{1.94}S$ is monoclinic, with lattice parameters of *a*=26.897, *b*=15.745, *c*=13.565 Å, α=90°, β=90.13°, γ=90°. At temperatures above 125 °C, $Cu_{1.94}S$ has only 85% of the copper sites occupied in the hexagonally packed framework of sulfur atoms.[33] This makes the Cu atoms in $Cu_{1.94}S$ behave virtually like ''fluid'' as is supported by the fact that djurleite has a high ionic conductivity above 100 °C. Thus, djurleite is an ideal host for forming multinary semiconductors with unique physical properties.[25] Gao *et al* have reported at an elevated reaction temperure of 200 °C and prolonged reaction time of 4-10 h, Sn atoms can be incorporated into the copper vacancy sites in $Cu_{31}S_{16}$ and transform the crystal lattice of $Cu_{31}S_{16}$ to give rise to the orthorhombic phase Cu_3SnS_4.[25] Thus, with even higher reaction temperature (260°C) and obviously much faster cation exchange process, orthorhombic Cu_4SnS_4 could be obtained in our experiment. Similar cation-exchange-induced phase transformations with a growth model of binary Cu−S to ternary Cu−Sn−S to quaternary Cu−Zn−Sn−S has also been reported by Tan *et al*.[34]

The crystal structure of $Cu_{1.94}S$ is quite complex, containing 32 sulfur atoms and 62 copper atoms in a unit cell. It should be noted that most of the Cu atoms (88.7%) have three coordination, 8% of Cu have four coordination and 1.6% of Cu have two coordination. Since Cu atoms with coordination less than four are not stable at higher temperatures, Sn will diffuse into the unit cell of $Cu_{1.94}S$ with partially replacement of Cu with increasing reaction temperature. During this process, the symmetry of the unit cell increases, thus the lattice parameters of Cu_4SnS_4 (*a*=13.57, *b*=7.69, *c*=6.42 Å) is about half of $Cu_{1.94}S$ (*a*=26.897, *b*=15.745, *c*=13.565 Å). Furthermore, the ionic radius of Sn^{4+} (55 pm for CN=4) is smaller than that of Cu^{+} (60 pm for CN=4), making the diffusion of Sn and replacement of Cu occur easily. While Sn and Cu adopt different valence states and coordination, it is not a simple replacement, but with simultaneous dissolution of Cu atom.

As can be seen from Table 1, the unit cell of Cu_4SnS_4 is closely related to that of $Cu_{1.94}S$. The β angle for djurleite $Cu_{1.94}S$ is only 90.13°, which is quite close to 90° for

orthorhombic Cu_4SnS_4, making the structural transformation from monoclinic $Cu_{1.94}S$ to orthorhombic Cu_4SnS_4 occur quite readily.

Based on the octet rule, if the sum of the valence electrons, ∑, of the cations surrounding an anion divided by the anion's coordination number plus the number of the anion's valence electrons is equal to eight, then that structure will be in a low energy state because the anion is in a closed-shell state.[35] In the orthorhombic structure of Cu_4SnS_4, there are three different S sites, namely S(1), S(2), S(3), and the ratio of S(1): S(2): S(3) equals to 2:1:1. All of the S sites are surrounded by metal atoms (M, Cu and Sn) to form SM_4 or SM_5 clusters with different combinations. The ∑ values of S(1)-[4Cu, Sn], S(2)-[3Cu, Sn], and S(3)-[4Cu, Sn] clusters, are 8, 7, and 8, respectively for the orthorhombic structure of Cu_4SnS_4. Thus, the average sum of the valence electrons, ∑, dived by coordination number is equal to 1.64. This value plus the number of the anion's valence electrons (6) is equal to 7.64, which is less than 8, indicating that Cu_4SnS_4 in the orthorhombic structure is not a stable structure. Interestingly, we have observed that Cu_4SnS_4 will partially convert to Cu_2SnS_3 (a=5.413, b=5.413, c=10.824 Å; α=β=γ=90°) at higher reaction temperatures, which is consistent with the predicted result.

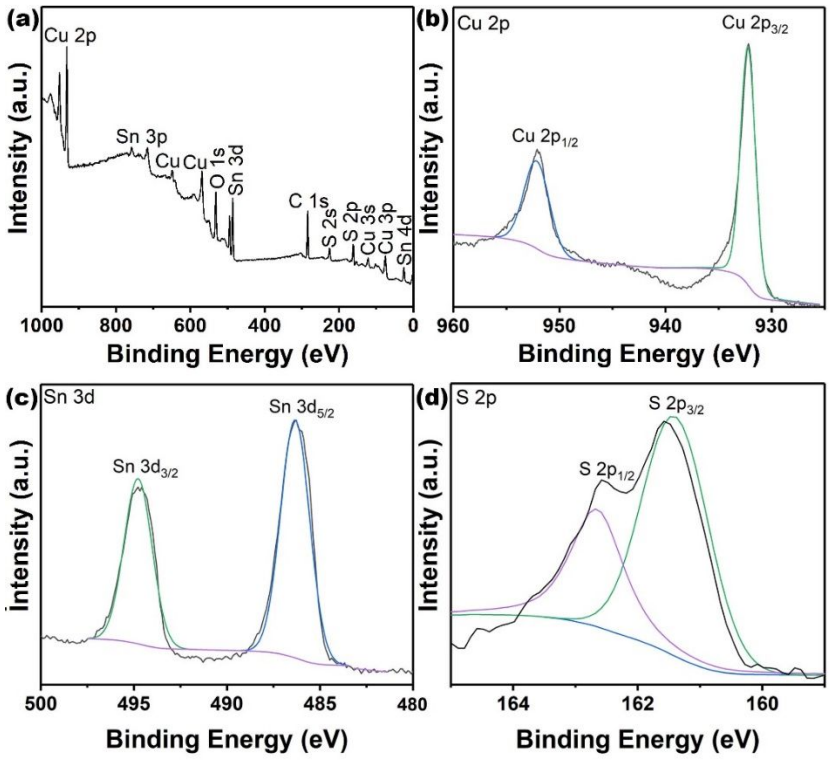

Fig. 4 (a) XPS survey spectrum, and high-resolution XPS spectra of (b) Cu, (c) Sn, and (d) S for Cu_4SnS_4 nanoplates.

X-ray photoelectron spectroscopy (XPS, Fig. 4) has been performed to confirm the oxidation states of elements Cu, Sn and S present in Cu_4SnS_4 nanoplates. The XPS peak software was used for the spectra calibration and data fitting. Fig. 4a displays the XPS survey spectrum of Cu_4SnS_4, which shows signals attributed to Cu, Sn, S, C, and O. High-resolution XPS spectra of Cu 2p, Sn 3d, S 2p, and O 1s have been measured to determine the oxidation states of these elements (Fig. 4b–d and Fig.S2). The peaks of Cu 2p appear at 932.2 eV ($2p_{3/2}$) and 951.9 eV ($2p_{1/2}$) with a separation of 19.7 eV, which is in accordance with the value of Cu (I). The high resolution XPS spectra of Sn shows two peaks at binding energies of 486.2 and 494.8 eV, which can be assigned to Sn (IV) with a peak separation of 8.6 eV. The sulfur was confirmed by peak splitting of 1.6 eV and two peaks located at 161.1 and 162.7 eV, which can be attributed to the presence of S^{2-}. The peak positions of Cu 2p, Sn 3d, and S 2p are in good agreement with literature reports.[17,18] No other valences, such as Cu(II), or Sn(II), are observed. As shown in Figure S2, the O 1s spectrum with a characteristic peak located at 532.0 eV could be de ascribe to the water molecule absorbed on the surface). [17,36]

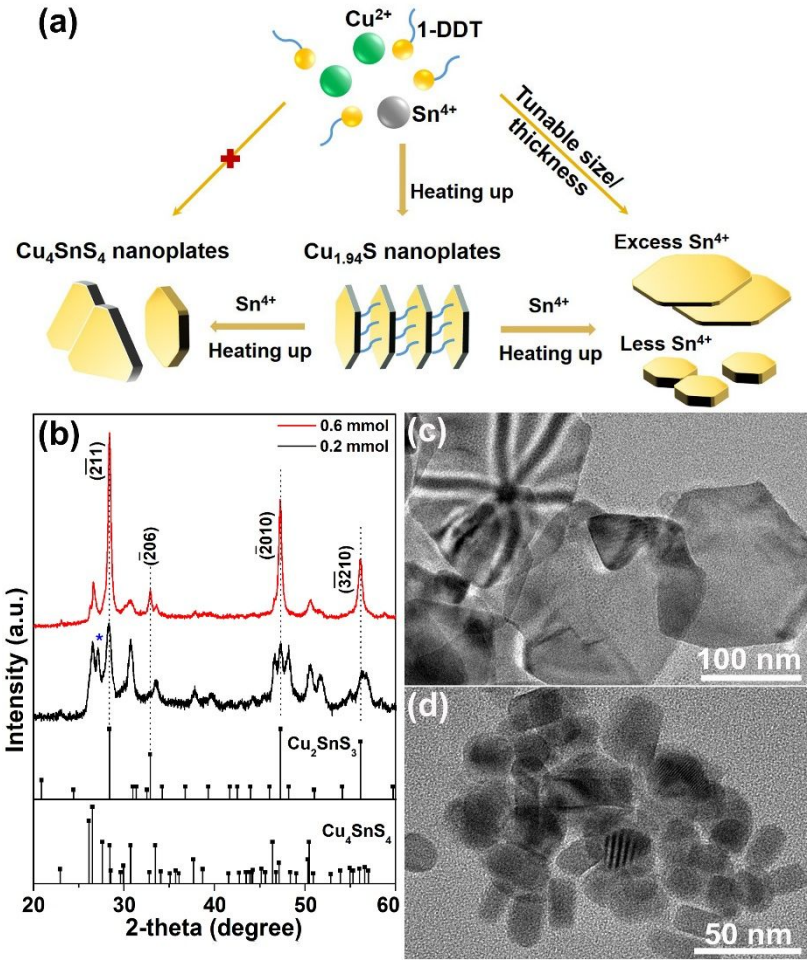

Fig. 5 (a) Illustration of the formation of Cu-Sn-S nanocrystals with tunable size and thickness, (b) XRD patterns, and (c,d) TEM images of Cu-Sn-S nanocrystals synthesized at 260 °C with different Sn precursor content of (c) 0.6 mmol and (d) 0.2 mmol.

We have found that the thickness and size of the as-synthesized nanoplates can be well controlled with different amount of $SnCl_4 \cdot 5H_2O$ precursor used for the reaction, as shown in Fig. 5a. As shown in Fig. 5b, with either less (0.2 mmol) or more (0.6 mmol) Sn precursor, the product obtained at 260 °C is composed of a mixture of Cu_2SnS_3 and Cu_4SnS_4 nanocrystals. With excess Sn precursor (0.6 mmol), the nanoplates are mainly composed of Cu_2SnS_3. More interestingly, with excess Sn precursor (0.6 mmol), larger nanoplates with lateral size of ~ 120 nm are obtained (Fig. 5c). As the crossection image of thin nanoplates is difficult to image using TEM, we are unable to obtain their exact thickness. Smaller nanoplates of ~25 nm in length and ~10 nm thickness are observed

when using 0.2 mmol $SnCl_4 \cdot 5H_2O$ as precursor (Fig. 5d). This might be due to the fact that when using 0.8 mmol $Cu(acac)_2$ as precursor, 0.2 mmol $SnCl_4 \cdot 5H_2O$ is just the exact amount based on stoichiometry for the formation of Cu_4SnS_4 nanocrystals. Thus, any extra available Sn precursor can act as shaping ligands resulting in the formation of nanoplates with larger lateral size. This observation is in accordance with our previous work on preparation of Cu_2ZnSnS_4 nanocrystals using $Cu_{1.94}S$ nanoplates as starting material. [26] However, changes in Sn concentration during the reaction can not only influence the morphology of the nanoplates but also the crystal structure. Thus, both the crystal structure and morphology are sensitive to the amount of Sn precursor used for the reaction.

During the synthesis of Cu_4SnS_4 nanoplates, we have maintained the reaction system at an intermediate temperature of 200 °C for 60 min to form the $Cu_{1.94}S$ nanoplates as initial seed nuclei. For comparison, controlled experiments have been done by directly increasing the reaction temperature from 120 °C to the reaction temperature (250, 260, and 270 °C) and maintained for 30 min. Interestingly, we notice that without the formation of $Cu_{1.94}S$ template, the product is composed of a mixture of Cu_4SnS_4 and Cu_2SnS_3 at reaction temperatures from 250 to 270 °C, as shown in supporting information Fig. S3. This indicates that the initially formed monoclinic $Cu_{1.94}S$ nanoplates aid in the formation of orthorhombic Cu_4SnS_4. Otherwise, the more stable phase Cu_2SnS_3 coexists with Cu_4SnS_4.

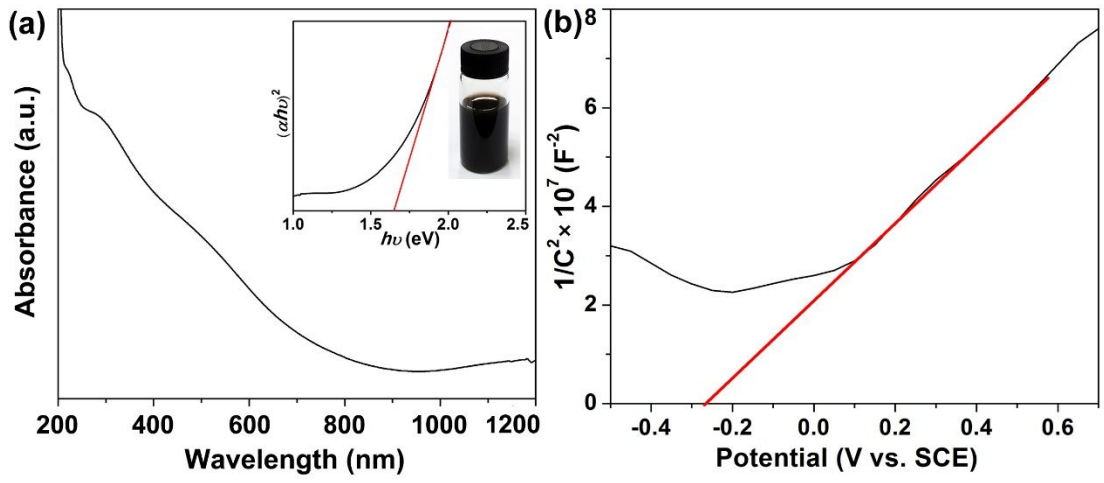

Fig. 6 (a) UV-vis spectroscopy of Cu_4SnS_4 synthesized at 260 °C, (b) Mott-Schottky

plot of Cu_4SnS_4 nanoplates electrode in aqueous solution of 0.1 M Na_2SO_4 at pH=7 obtained at the frequency of 1000 Hz.

It is well known that the band gap positions of the valence band (VB) and conduction band (CB) potentials are important for determining the photocatalysic properties of a semiconductor. We have used UV-vis spectroscopy and Mott-Schottky plot analysis to investigate the optical property and band potentials of the Cu_4SnS_4 nanoplates. The optical characteristics of as-synthesized Cu_4SnS_4 nanoplates has been studied by UV-Vis absorption spectroscopy (Fig. 6a). The as prepared Cu_4SnS_4 nanoplates exhibit board absorption in the visible region. The band gap is determined by plotting $(Ahv)^2$ versus hv (A=absorpance, h=Planck's constant and v=frequency) and extrapolating the linear portion of the spectrum in the band edge region. The band gap for Cu_4SnS_4 nanoplates is determined to be 1.65 ± 0.25 eV. The Cu_4SnS_4 nanoplates when dispersed in hexane and sonicated for 10 min forms a dark brown color solution, which indicates a strong absorption at visible wavelengths.

In order to determine the location of band edges of Cu_4SnS_4 nanoplates, we used the electrical impedance spectroscopy technique named Mott-Schottky analysis. The measurement of differential capacitance as a function of potential vs. SCE is performed in aqueous 0.1M Na_2SO_4 at pH=7 and frequency of 1000 Hz. As shown in Fig. 6b, the Mott-Schottky plot shows a positive slop, indicating n-type semiconducting behavior of Cu_4SnS_4. The flat-band potential can be estimated from the extrapolation of the linear portion in the plot of $1/C^2$ vs. potential (V) to the x-intercept, and is determined to be -0.26 eV vs. SCE and +0.19 eV vs. NHE. It is accepted that the flat-band potential is very close to the conduction band (CB) potential for n-type semiconductor.[37] Thus, the VB is about +1.84 eV with the band gap of 1.65 eV from UV-vis spectra.

In addition, the band gap positions of VB and CB potentials of Cu_4SnS_4 nanoplates have been calculated according to the following equations:[38,39]

$$E_{CB} = \chi - E_C - \frac{\mathrm{Eg}}{2} \qquad (1)$$

$$E_{VB} = E_{CB} + Eg \qquad (2)$$

Where E_{CB}, E_{VB}, χ, and E_g are the CB potential, VB potential, absolute

electronegativity, and band gap energy of the semiconductor, respectively. E_C is about 4.5 eV, which is the energy of free electrons on the hydrogen scale. The χ, calculated to be 5.16 eV, is the geometric mean of the absolute electronegativity of constituent atoms, for which the absolute electronegativity of copper, tin and sulfur is 4.48 eV, 4.30 eV, and 6.22 eV, respectively. The UV-vis spectra shows the band gap of Cu_4SnS_4 is about 1.65 eV. According to equations (1) and (2), the CB and VB potentials of Cu_4SnS_4 are determined to be -0.16 and +1.48 eV, respectively. Based on the calculated results, the electronic band structure of Cu_4SnS_4 can be obtained, as illustrated in Fig.7.

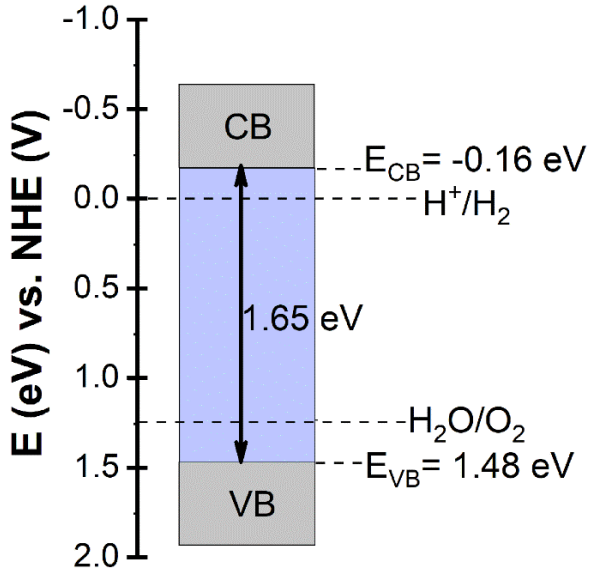

Fig. 7 Schematic illustration for the calculated electronic band structures of Cu_4SnS_4 nanoplates.

As noted that VB and CB potentials from the Mott-Schottky analysis are slightly higher than the calculated values. Thus, the relative locations of valence band (VB) maximum for Cu_4SnS_4 nanoplates was further determined via the XPS valence spectra. As displayed in Fig. 8, the Cu_4SnS_4 nanoplates has distinct VB with the edge of maximum energy at about +1.24 eV. Therefore, according to the band gap, the CB minimum of Cu_4SnS_4 nanoplates is -0.41 eV. As noted, the CB and VB potentials are somewaht sensitive to the measurements with a differential value of about 0.2-0.36 eV.

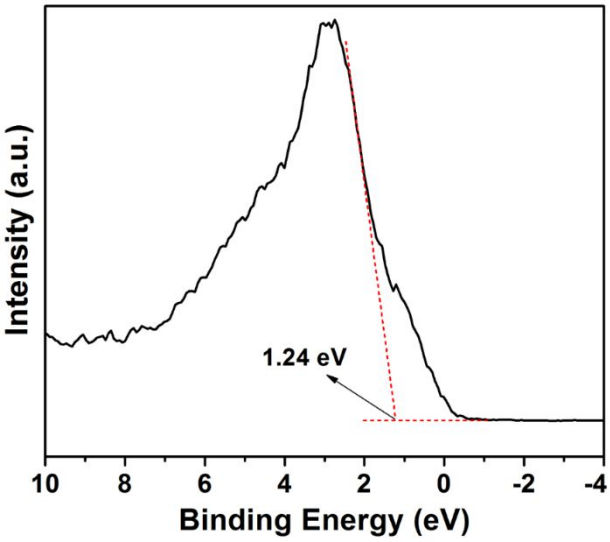

Fig. 8 Valence band (VB) XPS spectra of Cu_4SnS_4 nanoplates.

Conclusions

In summary, two-dimensional (2D) Cu_4SnS_4 nanoplates have been synthesized via a simple one-pot heat-up method using $Cu_{1.94}S$ nanocrystals as nuclei. The phase transformation monitored during the heating up process indicates that Sn^{4+} are gradually incorporated into the as-formed $Cu_{1.94}S$ nanoplates with increasing reaction temperature. Phase-pure Cu_4SnS_4 nanoplates are obtained at 260 ^oC for reaction time of 30 min. Our investigations also suggest that both the crystal structure and size of the nanoplates are dependent on the amount of Sn^{4+} used for the reaction. Excess Sn^{4+} aids in the formation of thinner and larger nanoplates, while less Sn^{4+} results in the formation of smaller and thicker nanoplates. Additionally, at higher reaction temperature (270 ^oC) or without the formation of $Cu_{1.94}S$ nuclei, the more stable Cu_3SnS_4 phase is formed during the reaction process. The as-prepared two-dimensional Cu_4SnS_4 nanoplates with band gap of ~1.65 eV and suitable electrical properties are attractive for photocatalytic applications. With earth-abundant and non-toxic composition, Cu_4SnS_4 has potential to be an environmentally-friendly photocatalyst. The synthesis strategy and findings will be relevant for the controllable synthesis of other copper chalcogenide nanocrystals as well as their photocatalytic applications.

Conflicts of interest

There are no conflicts to declare.

Acknowledgements

This research was supported by the National Natural Science Foundation of China (No. 51425202, No. 21506089), High-end Foreign Experts Project (GDW20173200136), and Natural Science Foundation of Jiangsu Province (BK20140929).

Notes and references

† Electronic Supplementary Information (ESI) available: XRD patterns with direct heat-up process. See DOI: 10.1039/x0xx00000x

1. C. Coughlan, M. Ibáñez, O. Dobrozhan, A. Singh, A. Cabot and K.M. Ryan, *Chem. Rev.*, 2017, **117**, 5865-6109.
2. C. Wu, Z. Hu, C. Wang, H. Sheng, J. Yang and Y. Xie, *Appl. Phys. Lett.*, 2007, **91**, 143104.
3. D. Avellaneda, M.T.S. Nair and P.K. Nair, *J. Electrochem. Soc.*, 2010, **157**, 346-352.
4. Y. Tan, Z. Lin, W. Ren, W. Long, Y. Wang and X. Ouyang, *Mater. Lett.*, 2012, **89**, 240-242.
5. Q. Chen, X. Dou, Z. Li, Y. Ni, J. Chen, F. Zhou, Y. Yamaguchi and S. Zhuang, *Optik.*, 2014, **125**, 3217-3220.
6. M. Umehara, Y. Takeda, T. Motohiro, T. Sakai, H. Awano and R. Maekawa, *Appl. Phys. Express*., 2013, **6**, 045501.
7. V.M. Dzhagan, A.P. Litvinchuk, M. Kruszynska, J. Kolny-Olesiak, M.Y. Valakh and D.R.T. Zahn, *J. Phys. Chem. C*, 2014, **118**, 27554-27558.
8. J. Lin, J-M. Lim, D.H. Youn, K. Kawashima, O-H. Kim, Y. Liu, O. Guo, O. Henkelman, O. Heller and C. B. Mullins, *ACS Nano*, 2017, **11***,* 10347.
9. H. Katagiri, K. Jimbo, W.S. Maw, K. Oishi, M. Yamazaki, H. Araki, A. Takeuchi, *Thin Solid Films*, 2009, **517**, 2455-2460.

10. I. D. Olekseyuk, I. V. Dudchak and L.V. Piskach, *J. Alloys Compd*., 2004, **368**, 135-143.
11. A. Lokhande, A. Patil, A. Shelke, P.T. Babar, M.G. Gang, V.C. Lokhande, D.S. Dhawale, C.D. Lokhande and J.H. Kim, *Electrochim. Acta*., 2018, **284**, 80-88.
12. A. Choudhury, S. Mohapatra, H.Y. Asl, S. H. Lee, Y. S. Hor, J. Medvedeva, D. L. McClane, G. E. Hilmas, M. A. McGuire, A. F. May, H. Wang, S. Dash, A. Welton, P. Boolchand, K. P. Devlin, J. Aitken, R. Herbst-Irmer and V. Petříček, *J. Solid State Chem.*, 2017, **253**, 192-201.
13. J. Lin, J-M. Lim, D. H. Youn, Y. Liu, Y. Cai, K.Kawashima, J-H. Kim, D-L. Peng, H.Guo, G. Henkelman, A. Heller and C. B. Mullins, ACS Nano, 2019, **13**, 10671-10681.
14. V. Maheskumar, P. Gnanaprakasam, T. Selvaraju and B. Vidhya, *Int. J. Hydrogen Energ.*, 2018, **43**, 3967-3975.
15. Y. Goto, Y. Kamihara and M. Matoba, *J. Electron. Mater.*, 2014, **43**, 2202-2205.
16. N. Nagasako, A. Suzumura and R. Asahi, *Acta Mater.*, 2019, **166**, 37-46.
17. X. Chen, X. Wang, C. An, J. Liu, Y. Qian, *J. Cryst. Growth*, 2003, **256**, 368-376.
18. Y. Chen, L. Ma, Y. Yin, X. Qian, G. Zhou, X. Gu, W. Liu, X. Wu and F. Zhang, *J. Alloy. Compd.*, 2016, **672**, 204-211.
19. A. Kassim, T. Tee, A.M. Sharif, D.K. Abdullah, M.J. Haron, H.S. Min, N. Saravanan, *J. Chil. Chem. Soc.*, 2009, **54**, 256-259.
20. U. Chalapathi, B. Poornaprakash and S-H. Park, *Sol. Energy*, 2017, **155**, 336-341.
21. M.T.S. Nair, C. Lopez-Mata, O. GomezDaza and P.K. Nair, *Semicond. Sci. Technol.*, 2003, **18**, 755-759.
22. X. Liu, X. Wang and M.T. Swihart, *Chem. Mater.*, 2015, **27**, 1342-1348.
23. X.-J. Wu, X. Huang, X. Qi, H. Li, B. Li, H. Zhang, *Angew. Chem. Int. Ed.*, 2014, **53**, 8929-8933.
24. X. Li, H. Shen, J. Niu, Y. Zhang, H. Wang and L. Li, *J. Am. Chem. Soc.*, 2010, **132**, 12778-12779.
25. L. Yi, D. Wang and M. Gao, *CrystEngComm*, 2012, **14**, 401-404.
26. X. Zhang, Y. Xu, C. Pang, Y. Wang, L. Shen, A. Gupta, N. Bao, *CrystEngComm*, **2018**, *20*, 2351-2356.
27. Y. Liu, M. Liu, D. Yin, W. Wei, P.N. Prasad and M.T. Swihart, *Chem. Mater.*, 2017, **29**, 3555-3562.
28. N. Bao, X. Qiu, Y-H.A. Wang, Z. Zhou, X. Lu, C.A. Grimes and A. Gupta, *Chem.*

Comm., 2011, **47**, 9441-9443.

29. X. Zhang, N. Bao, K. Ramasamy, Y-H.A. Wang, Y. Wang, B. Lin, A. Gupta, *Chem. Comm.*, 2012, **48**, 4956-4958.
30. J. Cardoso, C.A. Grimes, X. Feng, X. Zhang, S. Komarneni, M.V.B. Zanoni, N. Bao, *Chem. Comm.*, 2012, **48**, 2818-2820.
31. C. Zha, C. Ji, J. Zhang, L. Shen, X. Zhang, S. Dong and N. Bao, *RSC Adv.*, 2016, **6**, 107151-107157.
32. X. Zhang, Y. Xu, J. Zhang, S. Dong, L. Shen, A. Gupta and N. Bao, *Sci. Rep.*, 2018, **8**, 248.
33. M. Gao, B. Richter, S. Kirstein and H. Mohwald, *J. Phys. Chem. B*, 1998, **102**, 4096-4103.
34. J. M. R. Tan, M. C. Scott, W. Hao, T. Baikie, C. T. Nelson, S. Pedireddy, R. Tao, X. Ling, S. Magdassi, T. White, S. Li, A. M. Minor, H. Zheng and L. H. Wong, *Chem. Mater.*, 2017, **29**, 9192-9199.
35. H. Zhao, X. Xu, C. Li, R. Tian, R. Zhang, R. Huang, Y. Lyu, D. Li, X. Hu, L. Pan and Y. Wang, *J. Mater. Chem. A*, 2017, **5**, 23267-23275.
36. C. Shang, L. Hu, L. Fu, L. Huang, B. Xue, X. Wang, L. Shui and G. Zhou, *Solid State Ionics*, 2019, **337**, 47-55.
37. H. Mou, C. Song, Y. Zhou, B. Zhang and D. Wang, *Appl. Catal., B*, 2018, **221**, 565-573.
38. C. Lai, M. Zhang, B. Li, D. Huang, G. Zeng, L. Qin, X. Liu, H. Yi, M. Cheng, L. Li, Z. Chen and L. Chen, *Chem. Eng. J.*, 2019, **358**, 891-902.
39. J. Jin, J. Yu, D. Guo, C. Cui and W. Ho, *Small*, 2015, **11**, 5262-5271.